Mutual modulation between membrane-embedded receptor clustering and ligand binding in lipid membranes

ARTICLE *in* NATURE CHEMISTRY · DECEMBER 2010

Impact Factor: 25.33 · DOI: 10.1038/nchem.892 · Source: PubMed

2 AUTHORS:

Salvador Tomas
Birkbeck, University of London
34 PUBLICATIONS **606** CITATIONS
SEE PROFILE

Lilia Milanesi
Birkbeck, University of London
20 PUBLICATIONS **209** CITATIONS
SEE PROFILE

nature chemistry

ARTICLES

PUBLISHED ONLINE: 7 NOVEMBER 2010 | DOI: 10.1038/NCHEM.892

Mutual modulation between membrane-embedded receptor clustering and ligand binding in lipid membranes

Salvador Tomas* and Lilia Milanesi

Thanks largely to a cooperative chelate effect, clustered membrane-embedded proteins favourably bind to multivalent ligands in solution and, conversely, a multivalent receptor can induce the clustering of membrane-embedded proteins. Here, we use a chemical model to show that the binding of a monovalent ligand and the clustering of a membrane-embedded receptor are closely related processes that modulate each other without the contribution of any apparent multivalence effect. Clearly, the confinement of the receptor within the surface reveals cooperative effects between clustering and binding that are too weak to detect in bulk-solution systems. This work shows that for membrane-embedded receptors that undergo some degree of spontaneous clustering, analyses based on multivalence-mediated cooperativity are insufficient to describe fully the molecular recognition events induced by ligands in solution. Instead, a binding–clustering thermodynamic cycle is proposed for the analysis of the interaction of any kind of ligand with membrane-embedded receptors.

Membrane-embedded proteins provide the biomolecular machinery that regulates the contact between the cell and the external medium[1]. To a large extent, the mechanisms by which the regulation is achieved rely on changes in the organization of these proteins in response to changes in the environment. For example, signal transduction, which is at the heart of both the immunological response and neurotransmission, requires the association or clustering of membrane-embedded protein receptors[2,3]. The clustering is thought to be modulated by concomitant molecular recognition events, such as the assembly of surrounding lipids into rafts[4,5] that interact with the antigens[6,7] or the cytoskeleton[8,9]. Clearly, molecular recognition in and near lipid bilayers and, in particular, the interplay between the distribution of membrane-embedded receptors and in-solution ligands is at the heart of cellular function.

Simplified synthetic models, which traditionally are used to study molecular recognition phenomena in solution[10,11], can be used to elucidate the peculiarities of molecular recognition events near lipid bilayers and to create *de novo* biomimetic technology of increasing complexity[12]. Prominent contributions from the synthetic and supramolecular chemistry communities in the past two decades include the development of chemical approaches to study lipid–lipid interactions[13,14], embedded receptor–ligand interactions[15–17] and membrane adhesion and fusion[18–22], together with the development of biomimetic ion-channel systems for catalysis and sensing[23,24] and biomimetic vesicular systems based on block copolymers[25].

Stripped of all the biomolecular complexity, a chemical system that consists of a membrane, a membrane-embedded receptor and a ligand in solution has the appropriate level of complexity to allow the detailed study of emerging properties that result from the interplay between in-solution events (for example, receptor–ligand interactions) and in-membrane events (for example, receptor clustering)[26,27]. Most studies work on the assumption that binding of a ligand to a membrane-embedded receptor is modulated essentially by two factors: (1) the effect of the membrane interface environment on the binding affinity and (2) the impact of in-membrane receptor density on the multivalent effect when dealing with a multivalent ligand. For monovalent ligands, generally it is assumed that the apparent affinity does not depend on receptor density and that the ligand does not have an influence on the clustering of the receptor[15–17,22]. It is known, however, that monovalent ligands can modulate receptor clustering through, for example, a structural change in the receptor induced by the binding of the ligand[6], and that they also trigger the dispersion of clustered neutral receptors on binding of a charged ligand because of electrostatic repulsion between the receptor–ligand complexes[28]. In this work we use uncomplicated molecules based on a zinc metalloporphyrin as the model of membrane-embedded receptor, water-soluble nitrogen-containing molecules as ligands and unilamellar liposomes as model membranes to study in detail the relationship between receptor clustering and ligand binding in the absence of any apparent multivalency.

Results and discussion

Receptor clustering within the membrane. Porphyrin amphiphile **1** is ideally suited as a minimalist membrane-anchored receptor (Fig. 1). Cholesteryl moieties are used extensively as lipid-membrane anchors in artificial membrane receptors and their advantage over other anchor moieties is that they use a common component of biomembranes[15,29]. On the polar head group three ionized sulfonate groups force the porphyrin into the water–lipid interface and are known to induce a perpendicular orientation of the porphyrin ring relative to the lipid membrane[30]. The zinc metal centre provides the receptor with selectivity towards ligands that contain basic nitrogen, to yield complexes with moderate stability in aqueous media[31]. **1** was shown to form highly stable micellar assemblies in aqueous buffers (critical micellar concentration ~11 nM)[31]. The micellar aggregate presents ultraviolet–visible (UV-vis) and fluorescence spectra typical of porphyrin-aggregate species: the UV-vis spectrum in the Soret band region is broad, akin to that of porphyrin H aggregates, but

Department of Biological Sciences, School of Science, Birkbeck University of London, Malet Street, London WC1E 7HX, UK. *e-mail: s.tomas@bbk.ac.uk

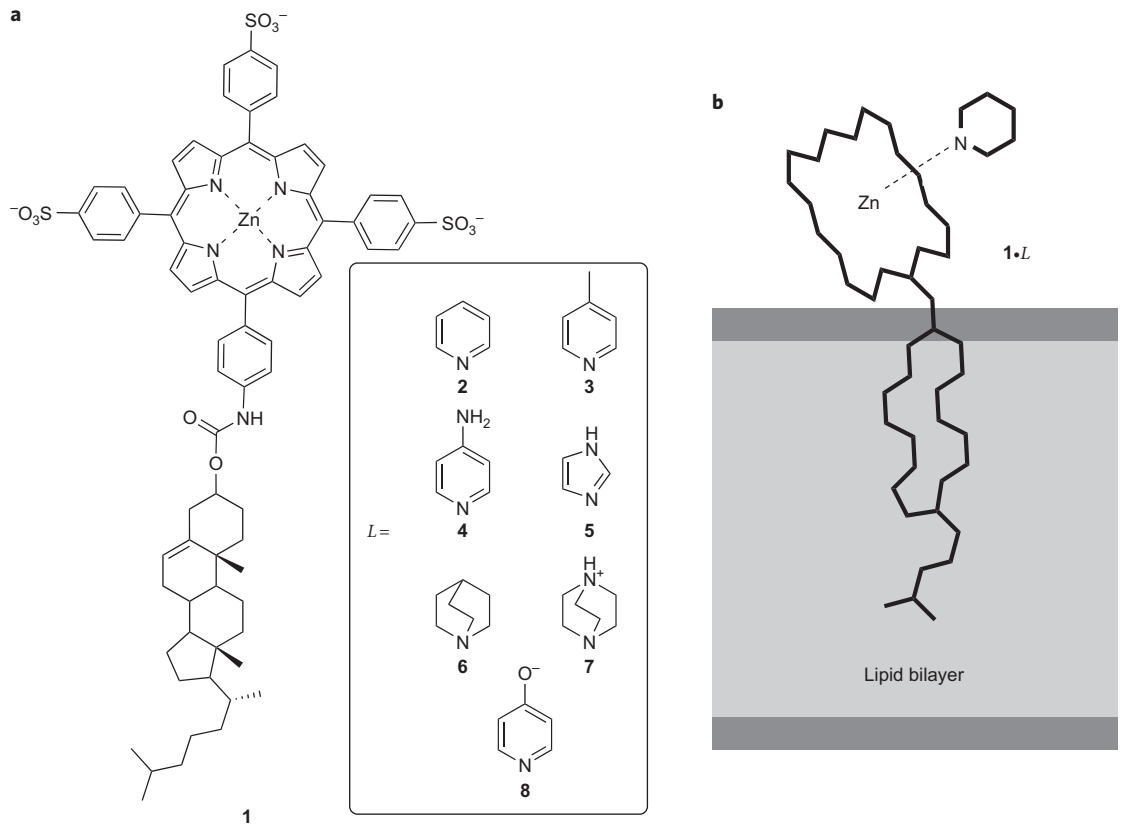

Figure 1 | Receptor and ligands. a, Chemical structure of receptor **1** and ligands *L* used in this work: **2**, pyridine; **3**, 4-picoline; **4**, 4-aminopyridine; **5**, imidazole; **6**, quinuclidine; **7**, 1,4-diazabicyclo[2.2.2]octane, a monoprotic ammonium cation; **8**, pyridin-4-olate. **b**, Representation of a complex of membrane-embedded **1** with a ligand *L*.

the fluorescence spectrum is quenched heavily. When **1** is mixed with liposomes its UV-vis spectrum becomes sharper and the fluorescence intensity increases. These changes are consistent with the dispersion of **1** micelles on incorporation into the lipid bilayer (Fig. 2a). Gel permeation chromatography (GPC) of liposome suspensions that contain **1** showed that **1** elutes together with the liposomes, consistent with the efficient embedding of **1** into the lipid bilayer. GPC traces of lipid suspensions prepared from different ratios $R_L = [\text{lipid}]/[\mathbf{1}]$ ($[M]/[\mathbf{1}]$), where $[M]$ is the concentration of lipid molecules, showed that the peak assigned to **1** micellar assemblies disappears for $R_L \geq 10$ (Fig. 3a). This observation gives an indication of the minimum relative amount of lipids necessary to incorporate **1** quantitatively into the liposomal membrane. Cryogenic transmission electron microscopy (cryo-TEM) experiments showed that for R_L values of 10 and 100 the appearance of the liposomal membrane was the same (Fig. 3b), so for these percentages of **1** the structure of the membrane was not perturbed dramatically.

For values of $R_L \geq 10$ the UV-vis and fluorescence spectra of **1**, however, changed with the relative amounts of lipid and **1**. For example, for a constant concentration of **1** at 1 μM, a change in R_L from 10 to 500 changed the UV-vis spectrum, which indicates the presence of two forms of **1** in an equilibrium that depends on the concentration of lipid (Fig. 2a, inset). The observed variations are consistent with either the formation of a bimolecular complex between **1** and the lipid molecules or the self-association of **1** within the membrane. By monitoring the spectral changes at different concentrations of **1** it became clear that they depend solely on the ratio R_L rather than on bulk concentrations of lipid and **1**, and thus can be assigned unequivocally to an in-membrane self-association process that involves a clustered form of **1** (*C*) and a dispersed form of **1** (*D*; see Supplementary Fig. 2).

Equilibria that involve bimolecular groupings of membrane molecules are used to analyse the clustering of membrane components[32]. However, the clustering of **1** in the membrane is not described well by bimolecular self-association models. Part of the problem is that the models implicitly assume that when a dimer is formed its molecules are no longer available for further association with the dispersed receptor. This scenario, which is an accurate description of self-association processes that involve the formation of a dimer through the use of specific intermolecular interactions or covalent bonds, may not be appropriate to describe the formation of weakly held clusters of molecules within a membrane. Instead, the formation of these clusters can be seen as the partition of **1** between two phases in the membrane: one phase is defined by the lipid molecules (*M*) and the other phase by **1** itself. Thus, individual molecules of **1** are either dissolved in *M*, and will therefore be in the dispersed form *D*, or dissolved in **1**, forming a cluster *C* of **1** molecules (*C* is of any size from two to *n* molecules). In other words, each individual **1** molecule is partitioned between a solvent consisting of lipid membrane molecules and a solvent consisting of other molecules of **1** (Supplementary Fig. 3). Importantly, from the point of view of each individual **1** molecule, the solvent defined by **1** is not just **1** in the *C* clustered form, but rather **1** in both *D* and *C* forms, because, by definition, the association of *D* with either a *C* (containing *n* molecules of **1**) or a second *D* molecule generates additional *C* (containing two molecules of **1**). In mathematical terms, this model is similar to nucleation–growth of polydisperse open oligomers, in which all the stepwise association constants are the same[33].

The equilibrium constant that relates the *C* and *D* forms of **1** is the partition coefficient of **1** between both solvents, K_{DC}. It can be shown (see Supplementary Information for details) that the

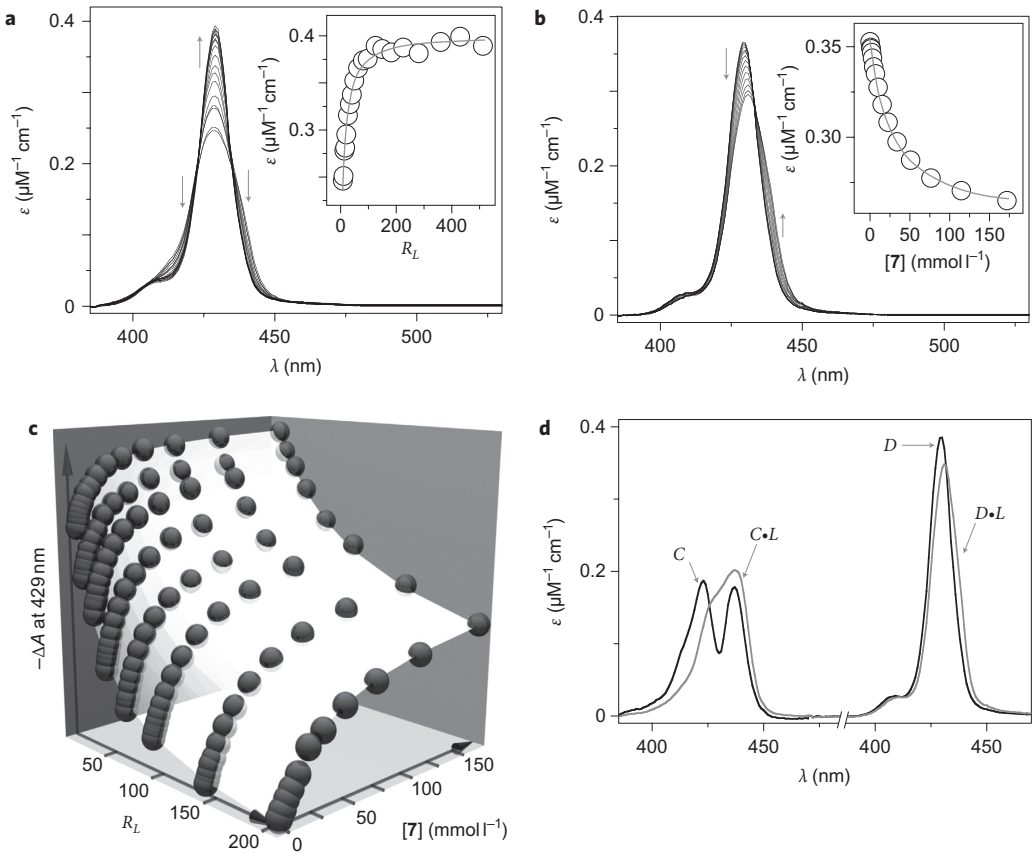

Figure 2 | Evaluation of receptor clustering and ligand binding. a, Changes in the Soret band region of the UV-vis spectra of lipid-embedded **1** with increase in R_L. The grey arrows indicate the direction of change. The inset shows the changes in absorbance at 429 nm (open circles) and the best fit to the clustering isotherm defined by equation (3) with $K_{DC} = 12 \pm 3$ (grey line). **b**, Changes in the Soret band region of the UV-vis spectra of lipid-embedded **1** at $R_L = 130$ on the addition of **7**. The grey arrows indicate the direction of change. The inset shows the changes in the extinction coefficient at 428 nm (open circles) and the best fit to a 1:1 binding isotherm (Supplementary equation (S9)) with $K_A = 38 \pm 4$ (grey line). **c**, Changes in absorbance (ΔA) at 429 nm with changes in R_L and concentration of **7** (dark spheres). The white surface is the best fit to the clustering–binding model using the program SPECFIT 3.0 (see Supplementary Table 2 and Supplementary Information for details). **d**, Soret band region of UV-vis spectra for the pure species ($L = \mathbf{7}$) derived from the global fitting procedure, using the program SPECFIT 3.0 (see Supplementary Information for details).

relationship between the bulk concentrations $[C]$ and $[D]$, the ratio of lipids R_L ($= [M]/[\mathbf{1}]$) and K_{DC} is:

$$K_{DC} = \frac{[C]R_L}{[D]} \tag{1}$$

This expression, given $R_L \gg [C]$, is equivalent to that of a bimolecular binding between the pseudospecies R_L and **1**. As we follow changes in the spectrum of **1**, the variation of the apparent molar extinction coefficient, ε_A, can be expressed as:

$$\varepsilon_A = \varepsilon_C x_C + \varepsilon_D x_D \tag{2}$$

where x_C and x_D are the fractions of the C and D forms, respectively, relative to the total amount of **1**, and ε_C and ε_D are the molar extinction coefficients of C and D. Combining equation (2) with mass balance and equation (1) we have the following expression for the clustering isotherm:

$$\varepsilon_A = \frac{\varepsilon_C K_{DC} + \varepsilon_D R_L}{K_{DC} + R_L} \tag{3}$$

which is analogous to that of a 1:1 binding for those cases in which one of the interacting partners is in large excess (here represented by $R_L \gg [C]$). From equation (1) it follows that the clustering constant K_{DC} corresponds to the ratio R_L at which 50% of embedded **1** is in the cluster form. Applying this model we find that $K_{DC} = 12 \pm 3$, that is when R_L is 12 (or when the percentage of **1** in the membrane is 7.1%), the concentration of **1** in the C and D forms is equal.

Ligand binding at the membrane interface. Nitrogen-bearing ligands can bind the zinc metal centre in the porphyrin moiety of **1** to form complexes of moderate stability in aqueous buffers[31]. For membrane-embedded **1** the binding affinity against a range of ligands was evaluated using UV-vis spectroscopy titration techniques (see Methods). The titration data fit well to a bimolecular binding isotherm for all the values of R_L and all the ligands tested (Fig. 2b). The apparent binding constant K_A for the formation of the receptor–ligand complex is, however, dependent on the value of R_L. The variation of K_A with R_L follows a similar trend for all ligands (see Supplementary Fig. 4). Changes in the local environment of the receptor make it reasonable to expect a different binding affinity towards the ligand from the clustered C and dispersed D forms of receptor **1**. The apparent binding constant K_A is the binding constant of the total **1** and the ligand L, that is $K_A = [\mathbf{1} \bullet L]/[\mathbf{1}][L]$, and can be expressed as a function of the corresponding D and C forms:

$$K_A = K_C x_C + K_D x_D \tag{4}$$

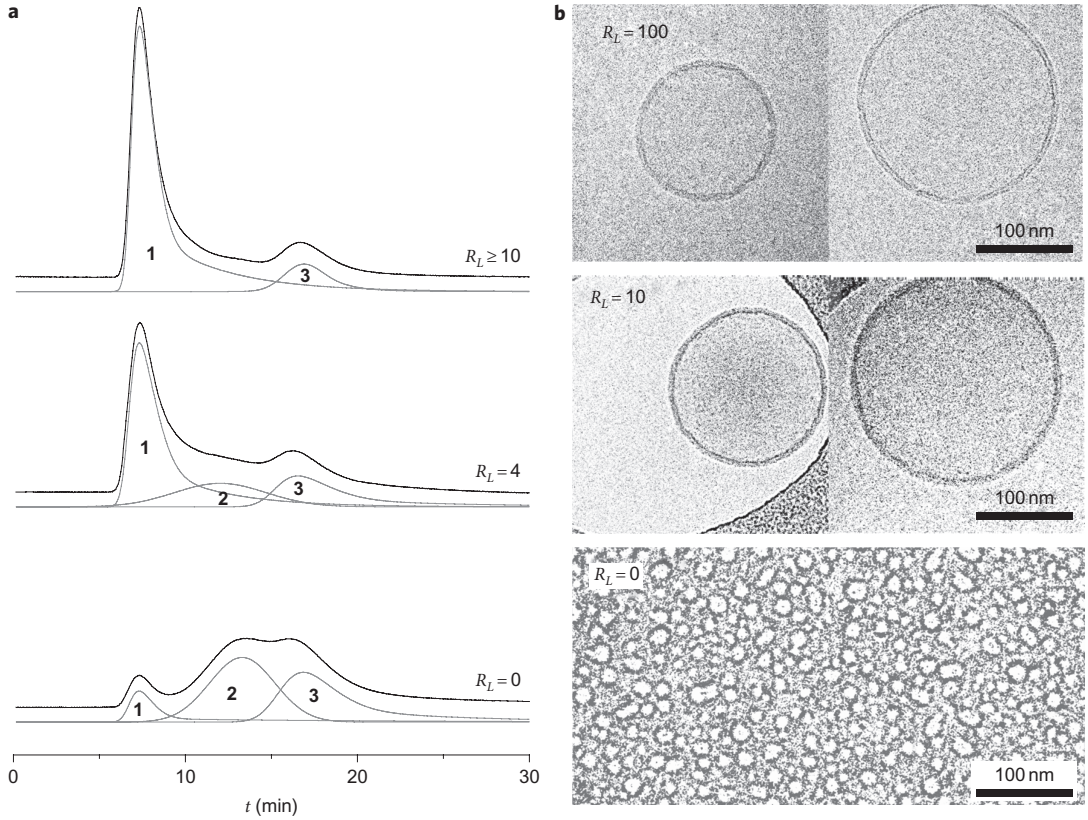

Figure 3 | Incorporation of the receptor in the lipid membrane. a, GPC traces at different [*M*]/[**1**] ratios, R_L. The black line represents the experimental chromatogram and the grey lines their deconvolution to the minimum number of component peaks. Up to three peaks were observed: peak 1 corresponds to species above the cutoff molecular weight of the media (500 kDa) and is assigned to aggregates of **1** micelles for $R_L = 0$ (no liposomes present) and to liposomes for $R_L = 4$ and $R_L \geq 10$; peak 2 is assigned to micellar assemblies of **1** (molecular weight ~70–100 kDa) and peak 3 is assigned to the retention peak of **1** caused by absorption into the media. **b**, Cryo-TEM images at different values of R_L.

Combining this with equation (1) gives:

$$K_A = \frac{K_C K_{DC} + K_D R_L}{K_{DC} + R_L} \quad (5)$$

Equation (5) is equivalent to the clustering isotherm for the spectroscopic variations (equation (3)) and it is consistent with the variations in K_A (see Supplementary Fig. 4).

When the changes of K_A with R_L are fitted to equation (5) and the previously determined K_{DC} is entered as a fixed parameter, it is possible to obtain values for K_D and K_C (see Supplementary Table 1). Knowing K_{DC}, K_C and K_D we can then determine the clustering constant of the ligand-bound form of the receptor, $K_{DCL} = [C{\bullet}L]R_L/[D{\bullet}L]$, which closes the ligand-binding and clustering thermodynamic cycle (Fig. 4a):

$$K_{DCL} = \frac{K_{DC} K_D}{K_C} \quad (6)$$

Values of K_{DCL} determined by completion of the cycle (using equation (6)) are, however, substantially different from K_{DCL} values estimated by fitting the spectral changes with R_L when an excess of ligand L is present using equation (3) (which is the final point of the ligand titrations, where most of the receptor is bound to L; see Supplementary Table 1). This lack of agreement is attributed to the oversimplification inherent in this model. Implicit in the derivation of equation (5) is the assumption that the molar fraction relative to the total receptor of the cluster and dispersed forms (x_C and x_D) does not change within a single titration experiment at a fixed R_L and that we can therefore assume only two coloured species, for example **1** and **1**•L, are present. In reality neither assumption is correct. As we have seen, the thermodynamic cycle requires that, if the binding affinities of the D and C forms of **1** for L are different ($K_C \neq K_D$), then the clustering tendency of **1** and **1**•L must also be different ($K_{DC} \neq K_{DCL}$). The implications are that the relative amounts of clustered and dispersed **1** change during the titration as the amount of ligand-bound receptor increases, and the spectral variations observed are the result of changing amounts of four coloured species (D, C, $C{\bullet}L$ and $D{\bullet}L$). It should be possible to determine a more precise set of binding parameters by taking into account the presence of these four species and the binding parameters that relate them (K_C, K_D, K_{DC} and K_{DCL}) when fitting the experimental spectral data. Clearly, the spectroscopic changes during a titration experiment at fixed R_L do not contain enough information to yield reliable values for all these parameters simultaneously, because, as we have seen, they fit well to a much simpler binding model that assumes the presence of only two coloured species and a single binding constant (see Supplementary equation (S9)). Instead, what is required is to fit all the spectroscopic data at different R_L values simultaneously to a global model. In this manner the effect of clustering (brought about mostly by changes in R_L) on binding (brought about mostly by changes in [L]) and *vice versa* are evaluated directly. We used the program SPECFIT 3.0 (ref. 34) to fit the spectral data in the Soret band region of the UV-vis absorbance spectra to a model that takes into account the presence of four coloured species (C, D, $C{\bullet}L$ and $D{\bullet}L$) related by three independent equilibrium constants (K_{DC}, K_C and K_D; see Supplementary Information for details). The value of K_{DC} derived from the analysis of the spectral data in the absence of L is entered as a non-adjustable parameter. The global fitting of the

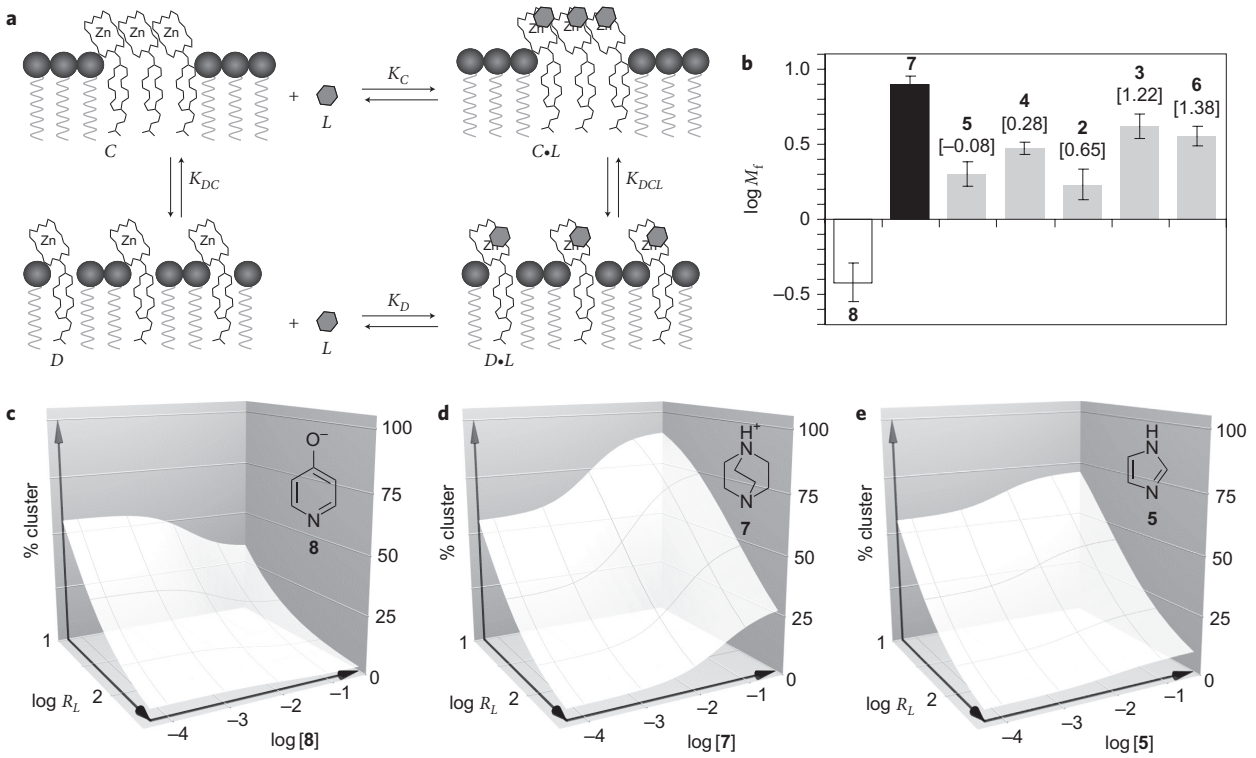

Figure 4 | Clustering–binding relationship and ligand modulation of the receptor clustering landscape. a, Schematic representation of the thermodynamic cycle described by the clustering and binding events. **b**, Graphical representation of the modulation factor M_f (represented here in the logarithmic form, log M_f) for the ligands used in this work. The error bar limits are set by $\log(M_f \pm ErM_f)$, with ErM_f twice the standard deviation, see Table 1. For the neutral ligands the value in brackets is the water–octanol partition coefficient, log P (values for **2**–**8** from the Interactive PhysProp Database Demo at http://www.syrres.com/esc/physdemo.htm). **c**–**e**, Modulation of the clustering landscape of **1** with changes in R_L and concentration of **8** (**c**), **7** (**d**) and **5** (**e**) shown as the variation of the percentage of **1** in the clustered form (that is, $C + C{\bullet}L$) (see Supplementary Information for details).

experimental data to this model is excellent (Fig. 2c and Supplementary Fig. 5).

Underpinning the validity of the model is that the Soret bands of all the coloured species derived from the fitting are consistent with the chemical structures of the different species: D and $D{\bullet}L$ have relatively sharp spectra, and C and $C{\bullet}L$ are broader, with features typical of porphyrin aggregates[31,35,36]. Also, the spectra of receptor–ligand complexes $C{\bullet}L$ and $D{\bullet}L$ show a red shift relative to the spectra of the free receptors, which is typical in zinc–porphyrin complexes with nitrogen-containing ligands (Fig. 2d and Supplementary Fig. 6). Finally, there is a remarkable agreement between the clustering constant of the ligand-bound receptor, K_{DCL}, calculated from the fitting of the ligand-saturated spectra using equation (3) and K_{DCL} derived from the global fitting using equation (6) (Table 1).

Clustering-binding mutual modulation. We define the modulation factor M_f as the ratio between the C and D forms of the ligand–receptor binding constants ($M_f = K_C/K_D$), which is equivalent to the ratio of the clustering constant of the ligand-bound and free forms of the receptor ($M_f = K_{DCL}/K_{DC}$). Therefore, M_f can be seen equally as the binding modulation factor on receptor clustering or as the clustering modulation factor on ligand binding (Fig. 4b). In all cases M_f is not one, which shows that the monotopic ligand used is capable of modulating, to some extent, the clustering of the receptor and, conversely, that the clustering of the receptor does modulate the affinity for the ligand in solution. The ability of the ligand in solution to modulate the receptor-clustering landscape is shown clearly in Fig. 4c–e. The binding of **8**, a negatively charged ligand, inhibits the clustering of the membrane-embedded receptor (Fig. 4c). The binding of the positively charged **7**, however, induces the clustering of the receptor (Fig. 4d). Neutral ligand **5** also induces ligand clustering, albeit to a more limited extent relative to that induced by **7** (Fig. 4e). To explain comprehensively the differences in M_f between the different ligands requires an accurate knowledge of the structure of the complexes, which is beyond the scope of the present work. It is possible, though, to rationalize the most salient features of the observed variations of M_f from the chemical nature of **1** and the ligands.

First, Fig. 4c–e shows that the clustering landscape within the lipid bilayer is regulated by both the in-membrane density of receptors and the concentration of ligand in solution (that is, R_L and $[L]$). For **8** and **7** the effect on the clustering landscape is attributed readily to electrostatic factors[37,38]: the complex **1**•**8** is charged more negatively than free **1**, which thus increases the repulsion between the head groups and reduces the clustering tendency[28]. However, the complex **1**•**7** is charged less negatively than free **1** and the effect is the opposite: reducing head-group repulsion leads to an increase in clustering. Conversely, the modulation of ligand affinity caused by receptor clustering can also be explained in terms of electrostatic factors: a receptor cluster has a high density of negative charge, which reduces its affinity for negatively charged **8**, but enhances its affinity for positively charged **7**. For these receptors it can be argued that a sort of 'multivalency' is at play: the first interaction is that of the basic nitrogen with the zinc of the porphyrin, and the subsequent interactions are electrostatic ones between the charged ligand and the surrounding receptors. The rest of the ligands tested were neutral under the experimental conditions. Still, all of them displayed a cluster-modulation capability by encouraging the clustering of **1**, that is, $M_f > 1$ (Fig. 4e, Table 1). For these ligands, the positive clustering modulation can

Table 1 | Clustering and binding parameters.

L	2	3	4	5	6	7	8
K_C*	53±7.6	240±28	600±30	180±13	3600±280	170±10	26±8.3
K_D*	30±4.0	58±5.8	200±9.0	90±3.9	980±85	21±1.8	71±3.4
K_{DC}†	10±3.3	11±3.8	13±2.9	15±3.8	13±2.8	10±2.9	11±3.4
K_{DCL}‡	17±3.3	46±3.8	39±8.7	30±3.8	47±8.3	80±9.0	2.1±1.4
M_f	1.7±0.39	4.2±0.82	3.0±0.27	2.0±0.37	3.6±0.54	8.0±1.1	0.37±0.13
K_{DCL}§	15±3.7	27±5.8	39±6.9	24±6.3	36±8.3	54±8.9	3.8±1.7

Errors are twice the standard deviation. K_C and K_D units are M^{-1} and refer to moles of **1**. K_{DC} and K_{DCL} are non-dimensional. *Calculated with the global model, with K_{DC} calculated from the fitting of the UV-vis data entered as a fixed parameter. †Calculated from the fitting of the UV-vis data in the absence of ligand. Variations of the K_{DC} values determined from different experiments are the result of the small error in lipid concentration inherent to the preparation of the sample (see Supplementary Information for details). ‡Calculated using equation (6). §Calculated, using equation (3), from the fitting of the UV-vis data in the presence of an excess of ligand.

be attributed to the enhanced hydrophobicity of the complex receptor–ligand relative to the free receptor. In the free receptor the zinc metal is coordinated to a water molecule, which on binding is substituted by a relatively hydrophobic ligand. Conversely, the modulation of ligand affinity on receptor clustering can be attributed to the presence of relatively hydrophobic cavities between head groups of **1** in the *C* form that favour the binding of relatively hydrophobic ligands[31]. Consistent with this explanation is the observation that the most hydrophobic neutral ligands (that is, with the highest log *P*, namely **3** and **6** (values from the Interactive PhysProp Database Demo at http://www.syrres.com/esc/physdemo.htm)) are those with the highest M_f (Fig. 4b). Hitherto, the relationships between ligand binding and clustering of membrane-embedded receptors typically were linked to a chelate cooperativity effect inherent to multivalent ligands[15–17,22,37,39], with a few exceptions, notably the dispersion of clusters of neutral receptors on binding of a charged ligand[28].

Here we show that for membrane-embedded receptors, the confinement of the receptor reveals a cooperativity effect between monovalent ligand binding and receptor clustering that is not apparent when both ligand and receptor are in solution. The binding–clustering relationship is described well by an uncomplicated binding–clustering thermodynamic cycle that should be applicable to the binding of any ligand to a membrane-embedded receptor, regardless of its valence. This work also illustrates how chemical systems of increasing, but addressable, complexity can be used to deepen our understanding of much more complex biological systems[26,27].

Methods

Liposomes used in this work were composed of dimyristoylphosphatidylcholine (DMPC) and cholesterol in an 8:2 molar ratio DMPC:cholesterol and variable amounts of **1**, and were prepared by evaporating the relevant amounts of ethanolic stock solutions, suspending the residue in the appropriate buffer and extruding through polycarbonate filters (200 nm pore size). For clustering experiments, 15 liposome samples with R_L from 10 to 500 were prepared and their UV-vis or fluorescent spectra recorded. For titration experiments, 15 samples of liposomes at a constant R_L and increasing ligand concentration were prepared and their UV-vis spectra recorded. Titration and clustering experiments were performed at 303 K. For **2**, the solvent was phosphate buffer 10 mM, pH 7.2; for **3** and **5** the solvent was carbonate buffer 10 mM, pH 10.3; for **4**, **6** and **8** the solvent was phosphate buffer pH 12.3; for **7** the solvent was acetate buffer 10 mM, pH 4.8. The clustering constant K_{DC} determined in all different buffers was the same within the standard error of the mean. At the working pH the relative amount of ligand in the desired protonation form was ≥95% in all cases. Data were analysed using the program SPECFIT 3.0. For GPC we used a low-pressure liquid chromatography column packed with Sepharose 4B. For cryo-TEM, samples (3.5 μl) were loaded on freshly discharged (60 s) holey carbon Lacey grids (S166-3; Agar Scientific). The grids were blotted and plunged into liquid ethane to embed the samples in vitreous ice. Low-dose images were recorded on a 4,096 × 4,096 charge-coupled device Gatan camera at a magnification of 100,000 and between 1 and 3 μm underfocus with a Tecnai F20 FEG electron microscope operated at 200 kV and equipped with a Gatan cold stage.

Received 17 May 2010; accepted 20 August 2010; published online 7 November 2010

References

1. Luckey, M. *Membrane Structural Biology* (Cambridge Univ. Press, 2008).
2. Grakoui, A. *et al.* The immunological synapse: a molecular machine controlling T cell activation. *Science* **285,** 221–227 (1999).
3. Renner, M., Specht, C. G. & Triller, A. Molecular dynamics of postsynaptic receptors and scaffold proteins. *Curr. Opin. Neurobiol.* **18,** 532–540 (2008).
4. Simons, K. & Toomre, D. Lipid rafts and signal transduction. *Nature Rev. Mol. Cell Biol.* **1,** 31–39 (2000).
5. Allen, J. A., Halverson-Tamboli, R. A. & Rasenick, M. M. Lipid raft microdomains and neurotransmitter signaling. *Nature Rev. Neurosci.* **8,** 128–140 (2007).
6. Tolar, P., Hanna, J., Krueger, P. D. & Pierce, S. K. The constant region of the membrane immunoglobulin mediates B cell-receptor clustering and signaling in response to membrane antigens. *Immunity* **30,** 44–55 (2009).
7. Munoz, P. *et al.* Antigen-induced clustering of surface CD38 and recruitment of intracellular CD38 to the immunologic synapse. *Blood* **111,** 3653–3664 (2008).
8. Chichili, G. R. & Rodgers, W. Clustering of membrane raft proteins by the actin cytoskeleton. *J. Biol. Chem.* **282,** 36682–36691 (2007).
9. Wang, H. B., Bedford, F. K., Brandon, N. J., Moss, S. J. & Olsen, R. W. GABA(A)-receptor-associated protein links GABA(A) receptors and the cytoskeleton. *Nature* **397,** 69–72 (1999).
10. Oshovsky, G. V., Reinhoudt, D. N. & Verboom, W. Supramolecular chemistry in water. *Angew. Chem. Int. Ed.* **46,** 2366–2393 (2007).
11. Cockroft, S. L. & Hunter, C. A. Chemical double-mutant cycles: dissecting non-covalent interactions. *Chem. Soc. Rev.* **36,** 172–188 (2007).
12. Voskuhl, J. & Ravoo, B. J. Molecular recognition of bilayer vesicles. *Chem. Soc. Rev.* **38,** 495–505 (2009).
13. Zhang, J. B., Cao, H. H., Jing, B. W., Almeida, P. F. & Regen, S. L. Cholesterol–phospholipid association in fluid bilayers: a thermodynamic analysis from nearest-neighbor recognition measurements. *Biophys. J.* **91,** 1402–1406 (2006).
14. Regen, S. L. Lipid–lipid recognition in fluid bilayers: solving the cholesterol mystery. *Curr. Opin. Chem. Biol.* **6,** 729–735 (2002).
15. Doyle, E. L., Hunter, C. A., Phillips, H. C., Webb, S. J. & Williams, N. H. *J. Am. Chem. Soc.* **125,** 4593–4599 (2003).
16. Jiang, H. & Smith, B. D. Dynamic molecular recognition on the surface of vesicle membranes. *Chem. Commun.* 1407–1409 (2006).
17. Thomas, G. B. *et al.* Carbohydrate modified catanionic vesicles: probing multivalent binding at the bilayer interface. *J. Am. Chem. Soc.* **131,** 5471–5477 (2009).
18. Gong, Y., Ma, M., Luo, Y. & Bong, D. Functional determinants of a synthetic vesicle fusion system. *J. Am. Chem. Soc.* **130,** 6196–6205 (2008).
19. Richard, A. *et al.* Fusogenic supramolecular vesicle systems induced by metal ion binding to amphiphilic ligands. *Proc. Natl Acad. Sci. USA* **101,** 15279–15284 (2004).
20. Menger, F. M., Seredyuk, V. A. & Yaroslavov, A. A. Adhesive and anti-adhesive agents in giant vesicles. *Angew. Chem. Int. Ed.* **41,** 1350–1352 (2002).
21. Mart, R. J., Liem, K. P., Wang, X. & Webb, S. J. The effect of receptor clustering on vesicle–vesicle adhesion. *J. Am. Chem. Soc.* **128,** 14462–14463 (2006).
22. Mansfeld, F. M., Feng, G. Q. & Otto, S. Photo-induced molecular-recognition-mediated adhesion of giant vesicles. *Org. Biomol. Chem.* **7,** 4289–4295 (2009).
23. Sanchez-Quesada, J., Isler, M. P. & Ghadiri, M. R. Modulating ion channel properties of transmembrane peptide nanotubes through heteromeric supramolecular assemblies. *J. Am. Chem. Soc.* **124,** 10004–10005 (2002).
24. Litvinchuk, S. *et al.* Synthetic pores with reactive signal amplifiers as artificial tongues. *Nature Mater.* **6,** 576–580 (2007).
25. Christian, D. A. *et al.* Spotted vesicles, striped micelles and Janus assemblies induced by ligand binding. *Nature Mater.* **8,** 843–849 (2009).
26. Ludlow, R. F. & Otto, S. Systems chemistry. *Chem. Soc. Rev.* **37,** 101–108 (2008).
27. Lehn, J. M. From supramolecular chemistry towards constitutional dynamic chemistry and adaptive chemistry. *Chem. Soc. Rev.* **36,** 151–160 (2007).

28. Sasaki, D. Y., Waggoner, T. A., Last, J. A. & Alam, T. M. Crown ether functionalized lipid membranes: lead ion recognition and molecular reorganization. *Langmuir* **18,** 3714–3721 (2002).
29. Dijkstra, H. P. *et al.* Transmission of binding information across lipid bilayers. *Chem. Eur. J.* **13,** 7215–7222 (2007).
30. Lahiri, J., Fate, G. D., Ungashe, S. B. & Groves, J. T. Multi-heme self-assembly in phospholipid vesicles. *J. Am. Chem. Soc.* **118,** 2347–2358 (1996).
31. Tomas, S. & Milanesi, L. Hydrophobically self-assembled nanoparticles as molecular receptors in water. *J. Am. Chem. Soc.* **131,** 6618–6623 (2009).
32. Davidson, S. M. K. & Regen, S. L. Nearest-neighbor recognition in phospholipid membranes. *Chem. Rev.* **97,** 1269–1279 (1997).
33. Hunter, C. A. & Anderson, H. L. What is cooperativity? *Angew. Chem. Int. Ed.* **48,** 7488–7499 (2009).
34. Gampp, H., Maeder, M., Meyer, C. J. & Zuberbuhler, A. D. Calculation of equilibrium-constants from multiwavelength spectroscopic data. 4: model-free least-squares refinement by use of evolving factor-analysis. *Talanta* **33,** 943–951 (1986).
35. Pasternak, R. F., Francesc, L., Raff, D. & Spiro, E. Aggregation of nickel(II), copper(II), and zinc(II) derivatives of water-soluble porphyrins. *Inorg. Chem.* **12,** 2606–2611 (1973).
36. Ribo, J. M., Crusats, J., Farrera, J. A. & Valero, M. L. Aggregation in water solutions of tetrasodium diprotonated meso-tetrakis(4-sulfonatophenyl) porphyrin. *J. Chem. Soc. Chem. Commun.* 681–682 (1994).
37. McLaughlin, S. & Murray, D. Plasma membrane phosphoinositide organization by protein electrostatics. *Nature* **438,** 605–611 (2005).
38. Denisov, G., Wanaski, S., Luan, P., Glaser, M. & McLaughlin, S. Binding of basic peptides to membranes produces lateral domains enriched in the acidic lipids phosphatidylserine and phosphatidylinositol 4,5-bisphosphate: an electrostatic model and experimental results. *Biophys. J.* **74,** 731–744 (1998).
39. Boniface, J. J. *et al.* Initiation of signal transduction through the T cell receptor requires the peptide multivalent engagement of MHC ligands. *Immunity* **9,** 459–466 (1998).

Acknowledgements

We thank K.C. Thompson, P.M. King, N.H. Williams and C.A. Hunter for reading the manuscript and the Faculty of Sciences at Birkbeck, University of London, for funding. TEM was performed at the School of Crystallography, Birkbeck University of London, supported by a Wellcome Trust programme grant to H. Saibil.

Author contributions

S.T. planned the studies, performed the synthesis of **1**, performed the optical spectroscopy and GPC experiments, interpreted the data and co-wrote the manuscript. L.M. performed the cryo-TEM experiments and co-wrote the manuscript.

Additional information

The authors declare no competing financial interests. Supplementary information and chemical compound information accompany this paper at www.nature.com/naturechemistry. Reprints and permission information is available online at http://npg.nature.com/reprintsandpermissions/. Correspondence and requests for materials should be addressed to S.T.